Molecular Dynamics Study of Two-Phase Flows

ME 346B Final Project Report

Filip Simeski and Suhas Jain Suresh

September 12, 2020

1 Introduction

Many engineering applications and natural phenomena require accurate understanding and treatment of interfaces between difference phases of matter. Whether one is interested in capillary flows in porous media, blood flow with suspension of blood cells or lubrication, at the interface between two phases there is a big separation in scales which introduces multiphysics and geometric complexities [10].

The velocity boundary condition across a solid-fluid interface has been especially debated, despite more than a century of study of this problem [4, 9]. This condition defines the transfer of tangential momentum. Most engineering problems are solved by assumption of no-slip velocity on the wall, but in cases such as moving contact line (MCL) this boundary condition breaks down [10, 6]. There have been advocates for slip boundary conditions since Navier [3] and Maxwell [2], but these models assume constant slip length which experimentally has been proven to be incorrect.

In this project we use MD simulations to support the unified slip boundary condition as proposed by Thalakkottor and Mohseni [7]:

$$U_s = L_s \delta \cdot \nabla \mathbf{u} \cdot \mathbf{s} \tag{1}$$

where U_s is the slip velocity, L_s is the slip length, δ is the unit direction vector of incident fluid molecules, $\mathbf{u}$ is the fluid velocity adjacent to the wall and $\mathbf{s}$ is the wall-tangent unit vector. This relation is based on previous work by Thompson and Troian [8], who showed that for single-phase Couette flow, the slip length and shear rate for a variety of conditions collapse on a single curve when properly scaled:

$$\frac{L_s}{L_s^o} = \left(1 - \frac{\dot{\gamma}}{\dot{\gamma}_c}\right)^{-1/2} \tag{2}$$

where L_s^o and $\dot{\gamma}_c$ are the asymptotic values of the slip length and the shear rate for the corresponding conditions.

We do this through two simple simulations: a single-phase Couette flow and a two-phase Couette flow. In addition to this we study two other problems which concern fluid flow in nanoconfined pores: nanodroplet in shearing flow between two plates and a sliding nanodroplet in a channel under the effect of a body force.

The rest of this report is organized as follows. In Section 2, we present the computational and simulation details, and define the problems. Then, in Section 3 we explain the findings through data analysis of the simulations described in the previous section. Finally, in Section 4 we summarize the key results and propose further directions for this study.

2 Methods and Problem Description

The simulations for this project are all run in LAMMPS with standard 12-6 Lennard-Jones potential (`pair_style lj/cut`). A cut-off radius of $r_c = 2.5\sigma$ is used. Fluids are maintained at temperature of $T = 1.1\epsilon/k_B$ with temperature rescale thermostat (`fix temp/rescale`). The thermostat enforces rescaling every 200 steps with window size of 0.02 and a fraction of 1. Each time step is 0.002 τ.

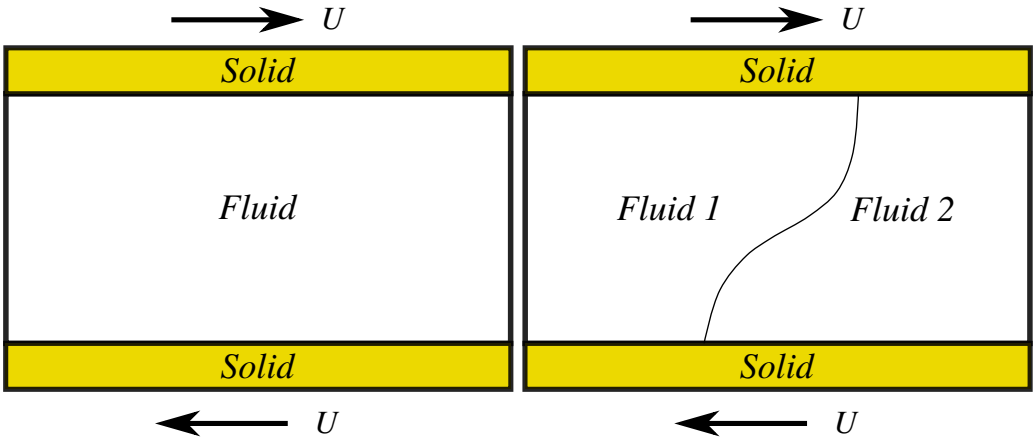

Figure 1: Schematic of the problems setup: Single-phase Couette flow (left), Moving contact line (right).

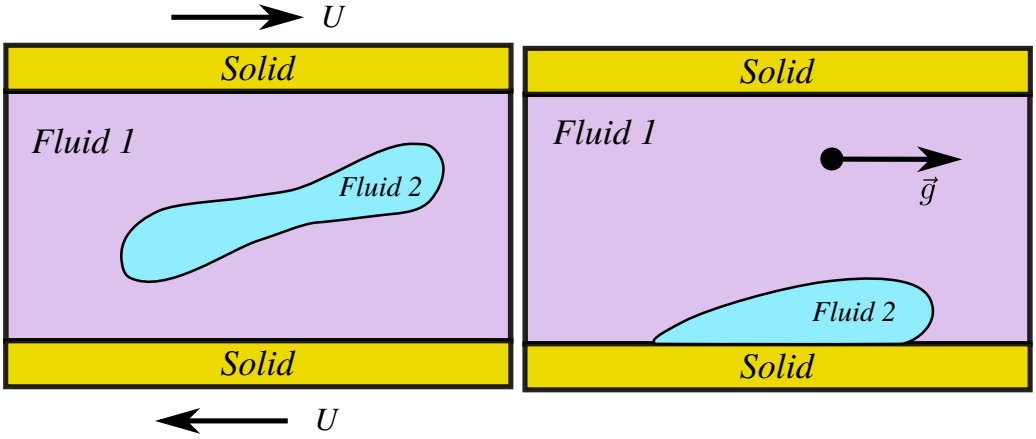

Figure 2: Schematic of the problems setup: Nanodroplet in a shearing flow (left), Sliding drop in a channel (right).

The problems we are trying to study are shown schematically in Fig. 1-2. An infinitely long channel is bounded by two parallel walls. The channel is periodic in x and z directions, and we use non-periodic and shrink-wrapped boundary condition in the y-direction. In the Couette flow problems (Fig. 1 and 2a) the walls are moving in opposite directions with constant velocity U. In the sliding drop problem, we are applying a uniform body force on all of the fluid in the x-direction.

For all problems, we use a domain size of $153\sigma \times 27.4\sigma \times 27.4\sigma$. Here there are total of 117,114 atoms, 81,153 of which are in the fluid and 35,961 in the solid walls. The number of atoms in the walls increases proportionally when we change the wall density. The fluid number density in all simulations is $0.73\sigma^{-3}$.

In problems where we define a wall velocity U, we vary this value to explore different applied shear rates on the fluid. The values of U studied are between 0.17 and 5.5 σ/τ. To prescribe this velocity to the solid walls, we use the `velocity` command. The velocity magnitude on both walls is equal, but its direction is opposite; with the top wall moving to -x and bottom wall moving to +x. We also use the `fix setforce` command to assign zero force on the walls, i.e. prevent wall-wall interactions or forces exerted from the fluid on the walls. In the sliding drop problem, where we apply a body force on the fluid, to study range of conditions we vary the body force magnitude to 0.01, 0.05, 0.1, 0.5 and 1 ϵ/σ. The body force is prescribed using the `fix gravity` command.

Finally, to explore wall-smoothness and effect of fluid wettability on slip length, we vary the unlike pair Lennard-Jones potential parameters for this problem. The droplet problems are studied only for the case 1 parameters. The parameters for the wall-fluid pair and fluid-fluid pair interactions are given in Table 3, where different cases corresponds to different slip lengths at the wall. Parameters $\epsilon^{f_1 f_2}$ and $\sigma^{f_1 f_2}$ are chosen such that the force between two fluids is purely repulsive, which results in preserving immiscibility of the two fluids.

Case	ϵ^{wf}/ϵ	σ^{wf}/σ	ρ^{w}/ρ	$\epsilon^{f_1f_2}/\epsilon$	$\sigma^{f_1f_2}/\sigma$
1	1.0	1.0	1.1	0.2	2.0
2	0.6	1.0	1.1	0.2	2.0
3	0.6	0.75	4.5	0.2	2.0
4	0.4	0.75	4.5	0.2	2.0

Table 1: Lennard-Jones parameters for wall-fluid (wf) and fluid-fluid (f_1f_2) interactions.

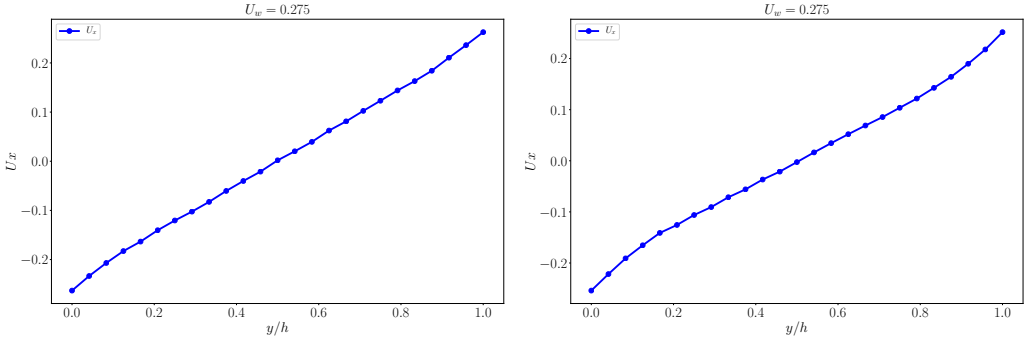

Figure 3: Averaged profiles of streamwise velocity as function of the wall normal coordinate for single-phase (left) and two-phase (right) Couette flow.

Each problem was post-processed differently depending on the quantities we were after. In the Appendix, we present representative temperature and pressure fluctuations for the simulations over time. These were extracted from the output file and directly plotted with no post-processing.

Next, for the single-phase and two-phase Couette flow the post-processing concerned the outputted velocities in the dump (trajectory) file. The domain was binned in the y-direction in 25 bins, and was averaged in the x- and z-directions. Moreover, the results of the fully-developed flow were also averaged over time to finally obtain a good statistically stable quantities. The x-velocity as function of y-coordinate obtained this way for case 1 is shown in Fig. 3. We could compare the velocity of fluid adjacent to the wall to the wall velocity to obtain the slip length according to

$$\Delta V = L_s \dot{\gamma} \tag{3}$$

In the simulations of a nanodroplet in shear flow between two plates, to study droplet deformation we used ImageJ [5]. This open-source software allows easy analysis of graphical images to obtain range of geometric values. In this case over ten frames from the fully-developed flow, we fitted an ellipse over the droplet and measured its major and minor axes. This data was averaged over for statistical significance. We report the droplet's aspect ratio as the ratio between the major and minor axes.

When measuring the front and rear contact angles in the sliding droplet simulations, we also used ImageJ. The front and rear contact angles are measured for each of ten frames from the fully-developed, steady-state flow and then averaged over. The results are presented as the mean value with the standard deviation representing the error bars in the next section.

3 Results and Discussion

The first step in our analysis was to show that using the Lennard-Jones parameters presented above, the fluids are truly immiscible, i.e. that they will form a sharp two-phase interface. To do this, we initialized a confined system with homogeneous mixture of Fluid 1 and Fluid 2 and ran an NVT simulation for 200τ. The visualization of the system at the initial and final states is shown in Figure 4. It is clear that the two phases coalesce and separate in the channel.

The next step is to measure the viscosity of the fluids. Both of them have the same viscosity since they interact with the same like-like type Lennard-Jones parameters and have the same mass. To do this, we set up a bulk system and sheared the fluid with constant shear rate of $0.01\tau^{-1}$.

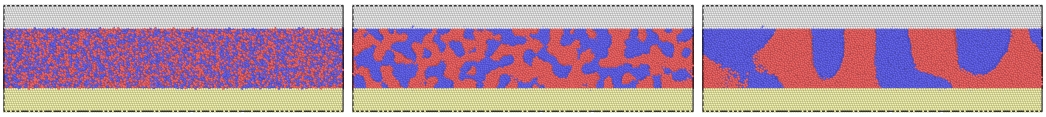

Figure 4: Homogeneous mixture of the two fluids would separate and coalesce.

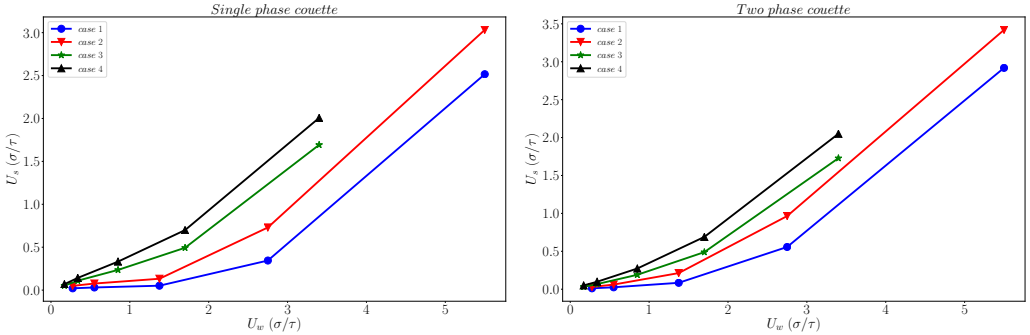

Figure 5: Dependence of slip velocity on wall velocity for single-phase (left) and two-phase (right) Couette flow. Each data point is one simulation.

Next, we analyze the shear stress fluctuations data to obtain the viscosity. To do this, we first define a stress integral:

$$\Sigma_{xy}(t) = \int_0^t \sigma_{xy}(t^{'})dt^{'} \tag{4}$$

which allows us to calculate the equivalent of the mean-square displacement for the stress integral

$$MSD_{\Sigma}(t) = \langle[\Sigma_{xy}(t) - \Sigma_{xy}(0)]^2\rangle \approx 2\mu t \tag{5}$$

where μ is the viscosity. Following this procedure, the viscosity is found to be $\mu = 2.17\epsilon\tau\sigma^{-3}$.

Now, we are finally ready to move to the simulations proposed in Section 2. For the simplest simulation, single-phase Couette flow, the first parameter we look at is the slip velocity (U_s) in the direction parallel to walls' velocity. As it can be seen in Figure 5, we notice that as we increase the wall velocity magnitude (U_w), the fluid slip velocity, U_s adjacent to the wall does not scale linearly. Since, binning is performed in the y direction to obtain the slip velocity of the fluid at the wall, we computed the standard error of the mean (SEM) and report them in Table **??**, to ensure statistical convergence of the data and to estimate the error associated with binning the data. The SEM values show that the data is statistically converged and the error values are quite small compared to the values of the mean.

	Moving contact line					Single-phase Couette Flow				
Case \ U_w	0.275	0.55	1.375	2.75	5.5	0.275	0.55	1.375	2.75	5.5
1	1.318	1.304	1.196	1.404	2.467	1.311	1.303	1.248	1.494	2.386
2	1.323	1.316	1.22	1.48	2.35	1.311	1.305	1.285	1.505	2.192
Case \ U_w	0.17	0.34	0.85	1.7	3.4	0.17	0.34	0.85	1.7	3.4
3	1.319	1.325	1.314	1.294	1.654	1.316	1.318	1.307	1.318	1.637
4	1.319	1.322	1.328	1.337	1.609	1.311	1.315	1.312	1.335	1.575

Table 2: Standard error of mean (SEM) in $\times 10^{-}3\sigma/\tau$ for the slip velocity at the wall for various values of wall velocity, U_w in σ/τ.

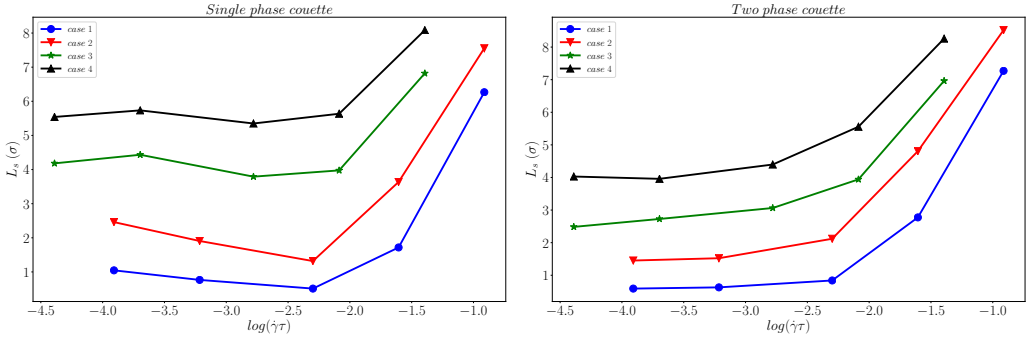

Figure 6: Dependence of slip length on shear rate for single-phase (left) and two-phase (right) Couette flow. Each data point is one simulation.

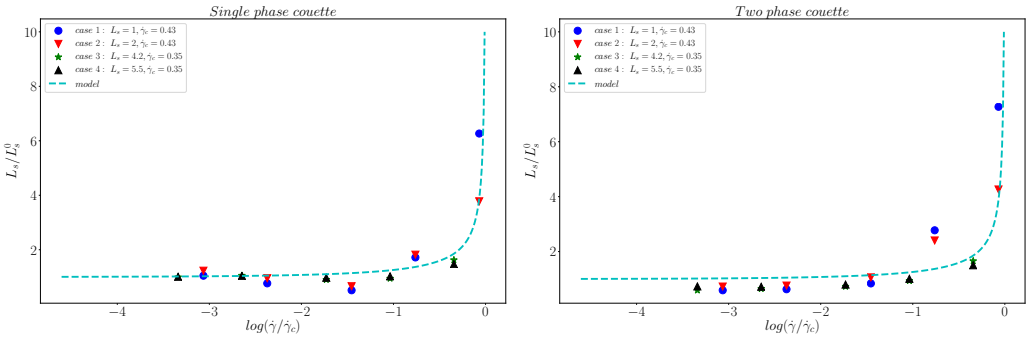

Figure 7: The universal scaling of Thompson and Troian applied to the data from Fig. 6. Better collapse of data for single-phase flow.

For this case, we also study the variation of slip length with shear rate. Compiling the data for various conditions and wall velocities (shear rates) on a single plot gives Fig. 6. We apply the Thompson and Troian model to see good collapse of the data as shown in Fig. 7. This allows us to conclude that there indeed is a universal scaling which defines a relation between the slip length and the shear rate as discussed in reference [8].

Increasing the simulation complexity, we next turn our focus to the problem of a two-phase Couette flow. Here we have a moving contact line along both the top and bottom walls. We follow the same post-processing methodology as in the single-phase simulations. Figure 6 shows the plot of the unscaled dependence of slip length on shear rate, while in Fig. 7 we present the scaled results according to the Thompson and Troian model. It is noted that in this case the agreement with the proposed law is less ideal than the agreement for a single-phase Couette flow. This is due to the dependence on the the streamwise spatial gradient of the wall-normal direction as discussed by Thalakkottor and Mohseni.

The final two configurations are simulations which were not studied by the study whose results we tried to replicate. However, we believed that these would be interesting extension to this work since they can represent problems in a variety of fields of study, most notably blood flows. The first setup shown in Fig. 2, concerns a droplet in shearing flow. In these simulations, since both fluids in this simulation have the same density and viscosity, the droplet would be neutrally buoyant. The shearing is done by assigning velocity to the walls varying from 0.275 to 5.5 σ/τ. The droplet which is placed in the center of the channel starts deforming under the influence of velocity gradients. To quantify this deformation, once it reaches steady state we fit an ellipse over it and report the aspect ratio of this fit. We did this procedure for ten frames extracted from the simulation, using ImageJ, and then averaged over this data.

In Fig. 8, it is noticeable that as we increase the wall velocity the drop gets more sheared up to wall velocity of $\approx$1.5 σ/τ, then the trend reverses. This goes in hand with the previous observations for the single-phase and two-phase Couette flow where it was observed that there is more slip as the wall velocity is increased. Note that in these simulations, while the droplet never breaks down due to shear along the channel's centerline, we do observe droplet break-up in the

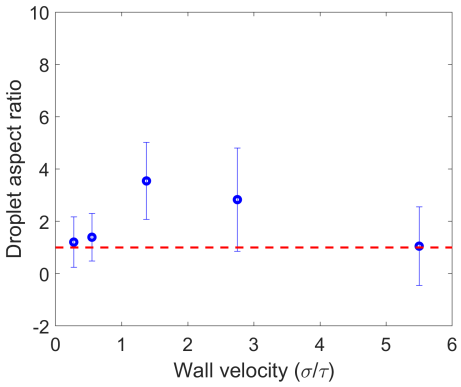

Figure 8: The aspect ratio of sheared nanodroplets in channel Couette flow field as function of wall velocity. The dashed line represents the aspect ratio of the droplets' initial state.

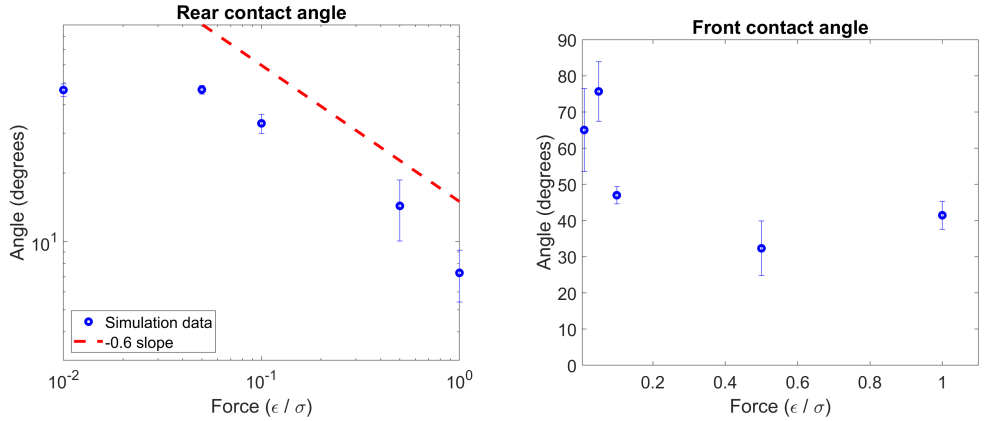

Figure 9: Rear (left) and front (right) contact angles of a neutrally-buoyant nanodroplet sliding due to a body force. Power-law dependence emerges for the rear contact angle.

case with the highest wall velocity. In this simulation, the drop drifts closer to the wall due to velocity field perturbations and enters the fast moving boundary layer which quickly causes it to break apart.

The last set of simulations explores the effect of a body force on the fluid has on a nano-droplet's front and rear contact angles. Once again, the droplet is neutrally buoyant. We apply a body force on both fluids in the +x direction. Physically this could represent the electric body force on charged particles or effect of a uniform pressure gradient among other examples. As explained in the previous section the body force absolute value is changed over two orders of magnitude.

The results shown in Fig. 9 are obtained with ImageJ. Both contact angles are defined as measured from the +x axis. It is interesting to note that while there is a very clear trend in the rear angle of the nanodroplet, the results for the front contact angle less conclusive. It is noticeable that the contact angle value in both cases decreases as we increase the applied body force in the fluid domain. Over the range of conditions studied, this relationship in non-linear. However, the relation can be fitted to a power-law with exponent of -0.6 for the rear contact angle.

4 Conclusion

We successfully implemented in LAMMPS two-phase fluid simulations confined in nanochannels to study a variety of fluid interface phenomena under a wide range of conditions. Based on the discussion in the previous sections, we can conclude that Molecular Dynamics simulations can be a very useful tool in studying interface problems and mechanisms. This approach could lay out the base for boundary condition definitions at the continuum scale.

We were able to observe similar trends as Thalakkottor and Mohseni (2016) for the slip length

in both single- and two-phase Couette flow. However, we extended this analysis to study two additional problems: nanodroplet in a shearing flow and a sliding nanodroplet. In the first of these two problems we observed that the relation between slip length and shear rate can be collapsed to a single curve for single-phase Couette flow. This universal scaling holds to some extent for two-phase Couette flow as well, however consideration of the wall-normal velocity is required for better collapse. During these simulations we observe that increasing wall velocity, would decrease the wall-normal gradient of the streamwise component of velocity. This goes hand in hand with the observations for a nanodroplet in a shear flow between two plates, where we showed that the droplet's aspect ratio can increase as much as 3.5, yet the droplet will not experience break up along the centerline since eventually the fluid near the walls starts slipping. Finally, in the problem of a sliding nanodroplet, we confirmed the intuitive result that a stronger force would extend the droplet more, decreasing the rear and front contact angles. While the front contact angle didn't change as significantly as hypothesized, we observed interesting power law behavior for the nanodroplet's rear contact angle.

References

[1] W. Cai and Y. Wang. Me346b. tutorial 13: Viscosity from stress fluctuation. 2019.

[2] J. C. Maxwell. The scientific papers of james clerk maxwell. 2:703–712, 1890.

[3] C. L. M. H. Navier. Memoirs de l'academie. *Royale des Sciences de l'Institut de France*, 1:414–416, 1823.

[4] S. Razavi, J. Koplik, and I. Kretzschmar. Molecular dynamics simulations: Insight into molecular phenomena at interfaces. *Langmuir*, 30(38):11272–11283, 2014.

[5] C. A. Schneider, W. S. Rasband, and K. W. Eliceiri. Nih image to imagej: 25 years of image analysis. *Nature Methods*, 9(7):671–675, 2012.

[6] J. H. Snoeijer and B. Andreotti. Moving contact lines: Scales, regimes, and dynamical transitions. *Annual Review of Fluid Mechanics*, 45:269–292, 2013.

[7] J. J. Thalakkottor and K. Mohseni. Unified slip boundary condition for fluid flows. *Physical Review E*, 94(2):023113, 2016.

[8] P. A. Thompson and S. M. Troian. A general boundary condition for liquid flow at solid surfaces. *Nature Letters*, 389:360–362, 1997.

[9] W.-M. Zhang, G. Meng, and X. Wei. A review on slip models for gas microflows. *Microfluidics and Nanofluidics*, 13(6):845–882, 2012.

[10] Y. Zhao. Moving contact line problem: Advances and perspectives. *Theoretical and Applied Mechanics Letters*, 4(3):034002, 2014.

Appendix

The viscosity calculation was done as described in the main body, following the procedure used in Tutorial 13 [1]. In Fig. 10 we present the stress integral as function of time.

In Fig. 11 we present sample temperature and pressure profiles for the simulations. As expected the both quantities oscillate, however we can easily notice the periodically repeating drop in temperature due to re-scaling.

The temperature rescaling was chosen as the approach for controlling the temperature since other thermostats were not working smoothly with the Lennard-Jones parameters used in this study. In Fig. 12, we show temperature and pressure of a simulation ran with Nose-Hoover thermostat. It can be seen that these are very similar to the fluctuations with the temperature rescale approach. However, by visual inspection of the particle trajectories it was observed that there was clustering of the fluid particles. We couldn't pin point the origin of this behavior.

Finally in Fig. 13 we show the output of the simulation with a Langevin thermostat. Unlike Figs. 11 and 12, here we do not see any fluctuations. This is behavior indicates that all the atoms are frozen, an observation which was confirmed with a visual inspection of the trajectory output.

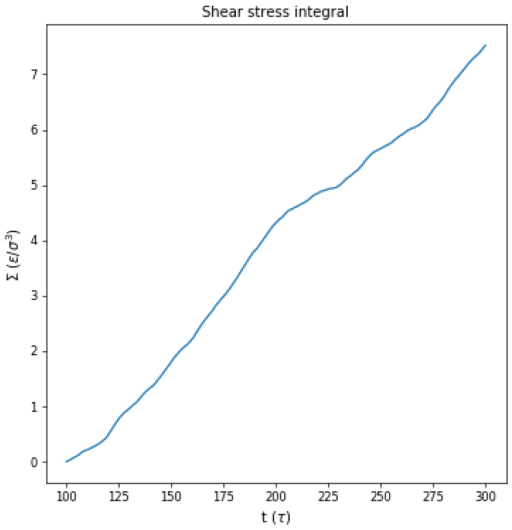

Figure 10: Stress integral as function of time. Reader is referred to the main body for the approach of calculating viscosity.

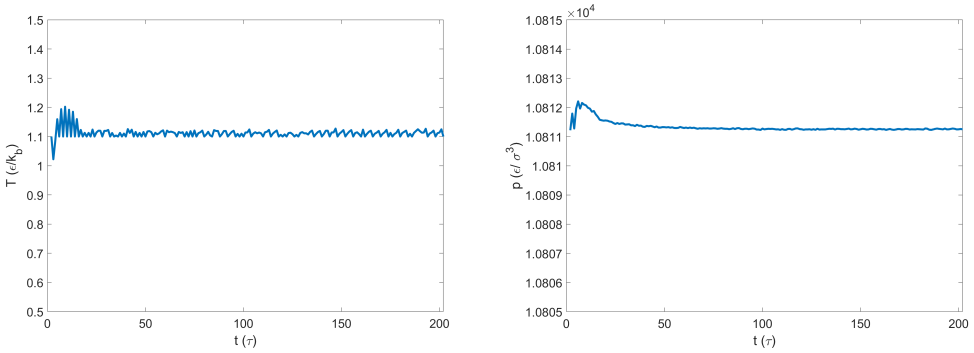

Figure 11: Temperature (left) and pressure (right) fluctuations. These are taken from the single-phase Couette flow with wall velocity of $U = 0.1\sigma/\tau$.

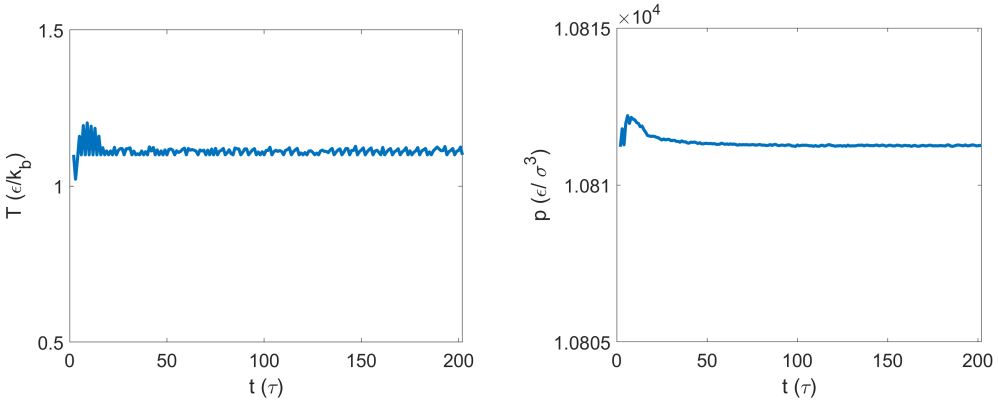

Figure 12: Temperature (left) and pressure (right) fluctuations with Nose-Hoover thermostat. These are taken from the single-phase Couette flow with wall velocity of $U = 0.1\sigma/\tau$.

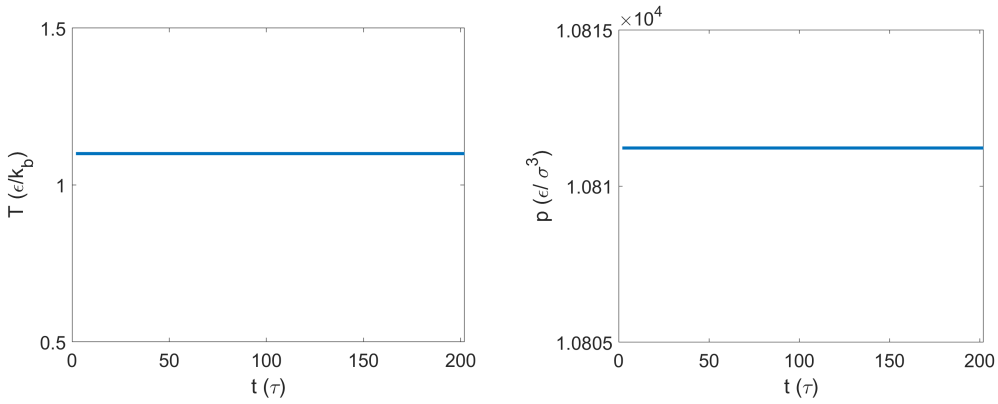

Figure 13: Temperature (left) and pressure (right) fluctuations with Langevin thermostat. These are taken from the single-phase Couette flow with wall velocity of $U = 0.1\sigma/\tau$.